Nonlinear and saturable absorption properties of PbS nanocrystalline thin films

Mustafa Yüksek[1*], Hüseyin Ertap[2], Mevlüt Karabulut[2], and Gasan M. Mamedov[2]

[1] *Department of Electrical-Electronics Engineering, Engineering and Architecture Faculty, Kafkas University, 36100 Kars Turkey*

[2] *Department of Physic, Science and Art Faculty, Kafkas University, 36100 Kars Turkey*

[*] *Corresponding author: mustafa_yuksek2001@yahoo.com*

Received March 18, 2013; accepted July 9, 2013; posted online September 3, 2013

The structural, morphological, optical, and nonlinear optical properties of a lead sulfide (PbS) thin film grown by chemical bath deposition (CBD) are investigated by X-ray diffraction (XRD), scanning electron microscope (SEM), ultraviolet-visible (UV-Vis), and open aperture Z-scan experiments. The band gap energy of the PbS nanocrystalline film is 1.82 eV, higher than that of bulk PbS at 300 K. The nonlinear absorption properties of the film are investigated using the open aperture Z-scan technique at 1064 nm and pulse durations of 4 ns and 65 ps. Intensity-dependent switching of the film from nonlinear absorption to saturable absorption is observed. The nonlinear absorption coefficient increases monotonically with increasing pulse duration from 65 ps to 4 ns.

OCIS codes: 300.1030, 310.6860.
doi: 10.3788/COL201311.093001.

Bulk lead sulfide (PbS) semiconductor crystals have an important direct narrow band gap energy (0.4 eV at 300 K) and a relatively large excitation Bohr radius of 18 nm[1]. These crystals are highly suitable for photography[2], solar control coating, diode laser, humidity and temperature sensor[3,4], and infrared detection[5] applications. In addition, PbS nanoparticles have exceptional third-order nonlinear optical properties and may be useful in optical devices, such as optical switches[6,7]. PbS exhibits a large blue-shift in its band gap energy as its particle size decreases due to the quantum confinement effect. Nanometer-sized semiconductor materials exhibit large third-order optical nonlinearity quantum sizes and interfacial effects[8,9]. Earlier studies have shown that reduction of the particle size of PbS to 2 nm results in increases in band gap energy to 5.4 eV[10,11], and this property has been widely investigated. Smaller particles can be obtained by nanoparticle and/or thin film technology. The third-order nonlinear optical properties of PbS nanoparticles have recently been studied using the femtosecond pump-probe technique[12], and these same properties of PbS-polymer nanocomposites have been studied through Z-scan experiments using femtosecond laser sources[8]. Thin film deposition methods widely used include thermal evaporation, sputtering, molecular beam epitaxy, chemical vapor deposition, spray pyrolysis, electrodeposition, and chemical bath deposition (CBD). The CBD method offers the following advantages over other techniques: 1) films can be deposited on all types of hydrophilic substrates; 2) the method affords a very simple and inexpensive process suitable for large-area deposition; 3) impurities in the initial chemicals can be made ineffective by complexation[13]. The electrical and optical properties of thin films can be changed depending on the deposition method[14−17]. In this study, a nanocrystalline PbS thin film is grown by CBD, and its saturable and nonlinear absorption properties are determined via the open aperture Z-scan technique using nanosecond and picosecond laser sources. This technique has recently been used to investigate the nonlinear absorption and refraction properties of some materials[18−20].

A PbS nanocrystalline thin film was deposited on a glass substrate by CBD. The substrate was cleaned for 1 h using a chromic acid solution ($K_2Cr_2O_7$:H_2SO_4) and then washed with doubly distilled water. The substrate was exposed to nitrogen gas to prevent native oxidation. The deposition bath consisted of 0.5 M lead acetate trihydrate, 1 M thiourea, 2 M sodium hydroxide, 1 M triethanolamine, and doubly distilled water. The substrate was immersed vertically into the deposition bath, and immersion was carried out for 120 min at 27 °C. The X-ray diffraction (XRD) pattern of the nanocrystalline PbS thin film was recorded in the 2θ range of 0° to 70° using an X-ray diffractometer (D/MAX-2200, RİAKU, Japan) with CuK_α radiation. The surface morphology of the film was studied by scanning electron microscope (SEM) using an SEM-LEO 440 microscope. The optical absorption spectrum of the PbS nanocrystal thin film was recorded between 500 and 1100 nm using a ultraviolet-visible (UV-Vis) absorption spectrophotometer (UV-1800, Shimadzu, USA). The thickness of the film was measured as 97 nm using a spectroscopic ellipsometer (M2000V, J. A. Woollam Co., USA). The saturable and nonlinear absorption of the PbS nanocrystalline thin film was measured using the open aperture Z-scan technique[21]. To determine the effects of mechanisms contributing to the nonlinear response of the film, nanosecond and picosecond laser sources were used for open aperture Z-scan experiments. One of the laser sources was a Q-switched Nd:YAG laser with pulse duration of 4 ns, wavelength of 1 064 nm (1.17 eV), and repetition rate of 10 Hz (Brillant, Quantel, England). The other laser source was a Q-switched Nd:YAG laser with a pulse duration of 65 ps, wavelength of 1 064 nm (1.17 eV), and repetition rate of 10 Hz (Leopard SV, Continuum, USA). The nanosecond and picosecond laser sources used

for the open aperture Z-scan experiments had Gaussian temporal profiles. To focus the lasers beams, a lens with a 20-cm focal length was used.

The XRD pattern of the PbS thin film is given in Fig. 1. Peak fitting of the figure was carried out, and the orientation, peak angles, lattice parameters, and crystalline sizes of the film are shown in Table 1. Figure 1 shows that the XRD pattern of the PbS thin film has two distinct peaks located at 26° (111) and 30° (200). Analysis of the XRD results indicates that the nanocrystals have a cubic structure belonging to the Fm-3m space group. The grain size of the nanocrystals was determined using the Scherrer equation, shown as

$$L = \frac{k\lambda}{B\cos\theta}, \tag{1}$$

where L is the grain size, k is the shape factor (0.5), λ is the wavelength of the X-ray used (0.15418 nm), B is the broadening of the line at half the intensity, and θ is the diffraction angle of the line under consideration.

The morphology of the PbS thin film is shown in Fig. 2, which illustrates that a nanocrystalline PbS thin film has grown on the substrate and that it does not have fissures or disturbances.

The optical absorption spectrum of the PbS nanocrystalline thin film is shown in Fig. 3. The gradual increase in band edge indicates the presence of defect states in the band gap. The energy band gap of the PbS nanocrystalline thin film was calculated based on the optical absorption spectrum (Fig. 3). To determine the energy band gap of the PbS nanocrystal thin film, $(\alpha h\nu)^2$ was plotted against $(h\nu)$, where α is the absorption coefficient and $h\nu$ is the photon energy (Fig. 3, inset). Interband absorption theory states that at the optical absorption edge, α varies with $h\nu$ according to Eq. (2)[22]:

$$(\alpha h\nu) = A(h\nu - E_{\mathrm{g}})^n, \tag{2}$$

where A is a constant and n is an index that can have values of 2, 3, 1/2, or 3/2, corresponding to allowed indirect, forbidden indirect, allowed direct, or forbidden direct transitions, respectively[22]. The band gap energy of the PbS nanocrystalline thin film is 1.82 eV, larger than the band gap energy of bulk PbS crystals (0.4 eV)[1]. The increase in band gap energy can be clearly attributed to the quantum confinement effect, since the grain size (Table 1) of PbS nanoparticles is smaller than the Bohr radius (∼18 nm) of the exciton in bulk PbS crystals.

Figures 4 and 5 respectively show the nanosecond and picosecond open aperture Z-scan measurements of the PbS nanocrystalline thin film. The PbS nanocrystalline thin film exhibits the same behavior under both nanosecond and picosecond pulse duration excitation, showing increases in low transmission with increasing intensity. Depending on the materials and/or pulse durations used, only one-photon absorption (OPA) contributions, only two-photon absorption (TPA) contributions, or their saturations are generally considered in Ref. [23]. Considering the defect states present in the band gap, in addition to the TPA effect, the OPA effect and the free-carrier absorption (FCA) effect contribute to nonlinear absorption. However, for larger intensities, the saturation effects of TPA, OPA, and FCA contribute to saturable absorption because of the filling mechanism of the defect states and conduction band.

To derive the transmission in the open aperture Z-scan

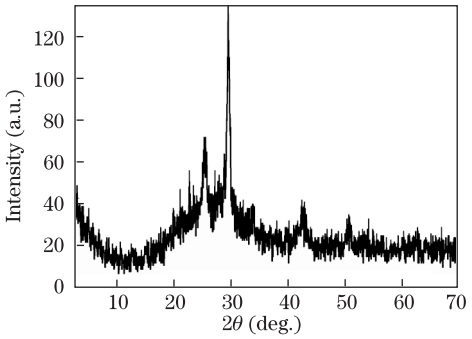

Fig. 1. XRD pattern of the PbS thin film deposited via the CBD technique.

Table 1. XRD Results of PbS Thin Film Deposited by CBD

Peak Number	2θ (deg.)	Orientation (hkl)	d (×10^{-10} m)	FWHM	Crystalline Size (nm)
1	26.012	1 1 1	3.424	0.688	11.6
2	30.047	2 0 0	2.965	0.492	16.2
3	43.015	2 2 0	2.097	0.089	9.04
4	51.363	3 1 1	1.788	0.234	13.7
5	53.525	2 2 2	1.712	0.09	9.07
6	62.475	4 0 0	1.482	0.09	9.16

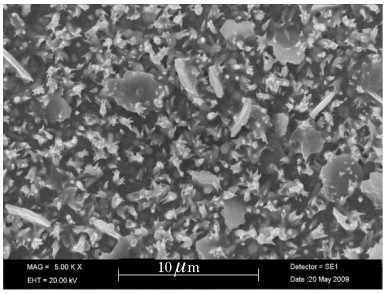

Fig. 2. SEM image of the PbS thin film.

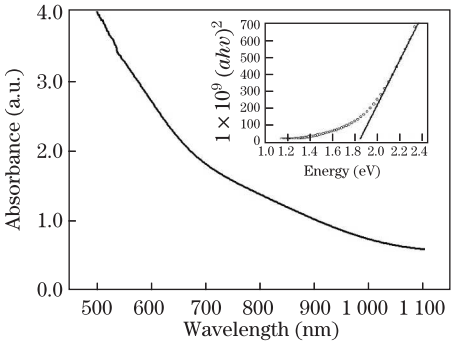

Fig. 3. Linear absorption spectrum of the PbS thin film. The inset shows the band gap of the film.

experiment, a model (given in Eq. (3)) incorporating OPA, TPA, FCA, and their saturations is used[24,25].

$$\frac{\mathrm{d}I}{\mathrm{d}z'} = -\frac{\alpha I}{1+I/I_{\mathrm{SAT}}} - \frac{\beta I^2}{1+I^2/I_{\mathrm{SAT}}^2} - \frac{\sigma_0 \Delta N I}{1+I^2/I_{\mathrm{SAT}}^2}, \tag{3}$$

where z' is the propagation distance inside the sample, α is the linear absorption coefficient, β is the TPA coefficient, σ_0 is the FCA cross section, ΔN is the photocarrier density, and I_{SAT} is the saturation intensity threshold for saturable absorption. The value of ΔN depends on both α and β absorption coefficients. To observe saturable absorption, the carrier lifetime (τ_0) can be increased well beyond the pulse durations used. In this case, the generated photocarrier density can be written as

$$\Delta N = \frac{\alpha \tau_0}{\hbar \omega_0} I. \tag{4}$$

Thus, Eq. (3) takes the form[24,25]:

$$\frac{\mathrm{d}I}{\mathrm{d}z'} = -\frac{\alpha I}{1+I/I_{\mathrm{SAT}}} - \frac{\beta_{\mathrm{eff}} I^2}{1+I^2/I_{\mathrm{SAT}}^2} = -f(I), \tag{5}$$

where

$$\beta_{\mathrm{eff}} = \beta + \frac{\sigma_0 \alpha \tau_0}{\hbar \omega_0}, \tag{6}$$

and ω_0 is the beam waist of the Gaussian spatial profile at focus. While the analytical solution of Eq. (5) is very difficult, the Adomian decomposition method[26] can be used to solve such saturable absorption problems for open aperture Z-scan theory[23,27]. According to the Adomian model, Eq. (5) can be integrated formally as

$$I_{\mathrm{out}} = I_{\mathrm{in}} - \int_0^L f(I)\mathrm{d}z, \tag{7}$$

where I_{in} is the input optical intensity to the front of sample, I_{out} is the exit optical intensity from the sample, and L is the thickness of sample. Using the fifth-order Adomian decomposition method[23,27], I_{out} can be expressed in terms of Adomian's polynomials. Therefore, the normalized transmittance can be expressed as a function of the sample relative position x[24,25]:

$$T(x,L) = \frac{\int_0^{\infty} I_{\mathrm{out}}(x,t) r \mathrm{d}r}{\mathrm{e}^{-\alpha_0 L} \int_0^{\infty} I_{\mathrm{in}} r \mathrm{d}r}, \tag{8}$$

where $x = z/z_0$ is the sample relative position, z is the sample position, $z_0 = \pi\omega_0^2/\lambda$ is the Rayleigh range, and λ is the wavelength of the laser used.

The data obtained from open aperture Z-scan experiments were fitted to the theory by treating I_{SAT} and β_{eff} as free parameters (Figs. 4 and 5). The results are given in Table 2. The thresholds of saturation intensity are 4.02×10^{11} and 2.14×10^{13} W/m^2 for nanosecond and picosecond excitation, respectively. Since the OPA depends on fluence, effects arising from OPA and contributing to the saturation are comparable for both nanosecond and picosecond excitation. High β_{eff} values are observed under nanosecond pulse duration excitation, which can be attributed to the fact that the contribution of FCA to saturation is greater than that of TPA. Thus, the saturation behavior takes place at lower saturation intensity values for nanosecond pulse durations than for picosecond pulse durations. When the pulse duration is decreased from 4 ns to 65 ps, the nonlinear absorption coefficient

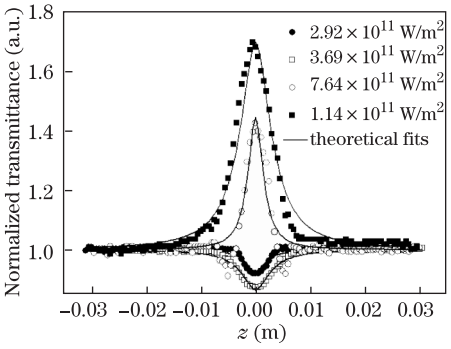

Fig. 4. Open-aperture Z-scan traces of the PbS thin film with nanosecond laser excitation under varying intensities.

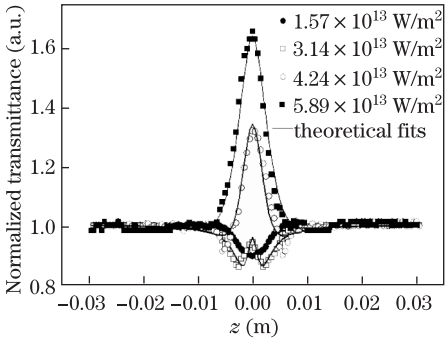

Fig. 5. Open-aperture Z-scan traces of the PbS thin film with picosecond laser excitation under varying intensities.

Table 2. Linear Absorption Spectrum and Open-Aperture Z-scan Results of PbS Thin Film Obtained under Nanosecond and Picosecond Laser Excitation and Varying Intensities

α	Thickness	Nanosecond Results		
(m^{-1})	(nm)	I_0 (W/m^2)	β (m/W)	I_{SAT} (W/m^2)
6.46×10^6	97	2.92×10^{11}	1.50×10^{-5}	4.02×10^{11}
		3.69×10^{11}	1.76×10^{-5}	
		7.64×10^{11}	2.63×10^{-5}	
		1.14×10^{12}	4.42×10^{-5}	
		Picosecond Results		
		I_0 (W/m^2)	β (m/W)	I_{SAT} (W/m^2)
		1.57×10^{13}	1.10×10^{-6}	2.14×10^{13}
		3.14×10^{13}	1.55×10^{-6}	
		4.24×10^{13}	2.35×10^{-6}	
		5.89×10^{13}	3.27×10^{-6}	

(β_{eff}) decreases monotonically. For nanosecond excitation, when the intensity increases from 2.92×10^{11} to 1.14×10^{12} W/m^2, the β_{eff} increases from 1.50×10^{-5} to 4.42×10^{-5} m/W. On the other hand, for picosecond excitation, when the intensity increases from 1.57×10^{13} to 5.89×10^{13} W/m^2, the β_{eff} increases from 1.10×10^{-6} to 3.27×10^{-6} m/W. Figures 4 and 5 show that the PbS thin film exhibits nonlinear absorption at low intensities and saturable absorption at high intensities. The increase in input intensity results in saturable absorption behavior because of the filling effect of localized defect states.

In conclusion, intensity-dependent switching of PbS nanocrystalline thin films from nonlinear absorption to saturable absorption is reported. The saturation intensity of the film is determined to be 4.02×10^{11} and 2.14×10^{13} W/m^2 for nanosecond and picosecond excitation, respectively. The materials show intensity-dependent switching, which may be used for optical pulse compression. For nonlinear optical investigations, PbS is generally used as nanoparticles; however, in this study, PbS is used as a thin film, which has been determined to be very useful material for technological applications.

References

1. J. L. Machol, F. W. Wise, R. C. Patel, and D. B. Tanner, Phys. Rev. B **48,** 2819 (1993).
2. P. K. Nair, O. Gomezdaza, and M. T. S. Nair, Adv. Mater. Opt. Electron. **1,** 139 (1992).
3. I. Pop, C. Nascu, V. Ionescu, E. Indrea, and I. Bratu, Thin Solid Films **307,** 240 (1997).
4. P. K. Nair, V. M. Garcia, A. B. Hernandez, and M. T. S. Nair, J. Phys. D Appl. Phys. **24,** 1466 (1991).
5. P. Gadenne, Y. Yagil, and G. Deutscher, J. Appl. Phys. **66,** 3019 (1989).
6. R. S. Kane, R. E. Cohen, and R. Silbey, J. Phys. Chem. **100,** 7928 (1996).
7. Y. Wang, Acc. Chem. Res. **24,** 133 (1991).
8. H. P. Li, B. Liu, C. H. Kam, Y. L. Lam, W. X. Que, L. M. Gan, C. H. Chew, and G. Q. Xu, Opt. Mater. **14,** 321 (2000).
9. B. Liu, H. Li, C. H. Chew, W. Que, Y. L. Lam, C. H. Kam, L. M. Gan, and G. Q. Xu, Mater. Lett. **51,** 461 (2001).
10. R. Thielsch, T. Böhme, R. Reiche, D. Schlafer, H. D. Bauer, and H. Böttcher, Nanostruct. Mater. **10,** 131 (1998).
11. K. K. Nanda, F. E. Kruis, H. Fissan, and M. Acet, J. Appl. Phys. **91,** 2315 (2002).
12. D. Li, C. Liang, Y. Liu, and S. Qian, J. Lumin. **122-123,** 549 (2007).
13. K. L. Chopra and I. Kaur, *Thin Film Device Applications* (Plenum Press, New York, 1983).
14. G. Micocci, A. Serra, and A. Tepore, J. Appl. Phys. **82,** 2365 (1997).
15. J. F. Sanchez-Royo, D. Errandonea, A. Segura, L. Roa, and A. Chevy, J. Appl. Phys. **83,** 4750 (1998).
16. S. Shigetomi, T. Ikari, and H. Nakashima, J. Appl. Phys. **80,** 4779 (1996).
17. G. M. Mamedov, M. Karabulut, A. O. Kodolbaş, and Ö. Öktü, Phys. Stat. Solid. B **242,** 2885 (2005).
18. A. J. Almosawe and H. L. Saadon, Chin. Opt. Lett. **11,** 041902 (2013).
19. M. Dezhkam and A. Zakery, Chin. Opt. Lett. **10,** 121901 (2012).
20. Y. Fan, Z. Jiang, and L. Yao, Chin. Opt. Lett. **10,** 071901 (2012).
21. M. Sheik-Bahae, A. A. Said, T. H. Wei, D. J. Hagan, and E. W. Van Stryland, IEEE J. Quantum Electron. **26,** 760 (1990).
22. J. I. Pankove, *Optical Process in Semiconductors* (Courier Dover Publications, New York, 1971).
23. B. Gu, Y. X. Fan, J. Chen, H. T. Wang, J. He, and W. Ji, J. Appl. Phys. **102,** 083101 (2007).
24. M. Yüksek, U. Kürüm, H. Gul Yaglioglu, A. Elmali, and A. Ateş, J. Appl. Phys. **107,** 033115 (2010).
25. U. Kürüm, M. Yüksek, H. Gul Yaglioglu, A. Elmali, A. Ateş M. Karabulut, and G. M. Mamedov, J. Appl. Phys. **108,** 063102 (2010).
26. G. Adomian, *Solving Frontier Problems of Physics*: *The Decomposition Method* (Springer, 1994).
27. B. Gu, Y. X. Fan, J. Wang, J. Chen, J. P. Ding, H. T. Wang, and B. Guo, Phys. Rev. A **73,** 065803 (2006).